Climatic impacts on an Arctic lake since 1300 AD: a multi-proxy lake sediment reconstruction from Prins Karls Forland, Svalbard

Orme, L.C.[1,2] (lisa.orme@mu.ie), Lind, E.M.[3,4] (ewa.lind@ivl.se), Holm, T.M.[5] (t-m-holm@online.no), Kjellman, S.E.[4,6] (sofia.e.kjellman@uit.no), Koinig, K.A.[5] (Karin.koinig@uibk.ac.at), Hormes, A.[6] (anne.hormes@uit.no), Rosqvist, G.C.[4] (ninis.rosqvist@natgeo.su.se), Ruppel, M.[7] (meri.ruppel@helsinki.fi), Divine, D.V,[2] (Dmitry.Divine@npolar.no), Husum, K.[2] (Katrine.Husum@npolar.no), Miettinen, A.[2,7] (arto.miettinen@helsinki.fi) & Isaksson, E.[2] (Elisabeth.isaksson@npolar.no)

[1] ICARUS, Department of Geography, Maynooth University, Maynooth, Ireland

[2] Norwegian Polar Institute, Tromsø, 9296, Norway

[3] IVL Swedish Environmental Research Institute, Stockholm, SE-100 31 Stockholm, Sweden

[4] Department of Physical Geography, Stockholm University, SE-106 91 Stockholm, Sweden

[5] Department of Ecology, University of Innsbruck, Austria

[6] Department of Geosciences, UiT The Arctic University of Norway, Postboks 6050 Langnes, NO-9037 Tromsø, Norway

[7] Ecosystems and Environment Research Programme, Faculty of Biological and Environmental Sciences, FI-00014 University of Helsinki, Finland

Corresponding author email: lisa.orme@mu.ie

Key words

Svalbard, Lake Sediments, Climate Change, North Atlantic Oscillation, XRF, Stable Isotopes

Abstract

On the remote Arctic archipelago of Svalbard, there is increasing evidence of environmental impacts from climate change. The analysis of lake sedimentary records can be used to assess how strongly these recent changes have altered lake ecosystems. Sediments deposited during the last millennium from Lake Blokkvatnet, Prins Karls Forland, were analysed using a multiproxy approach, including stable isotope and X-ray fluorescence (XRF) analysis. The results were interpreted as reflecting variability of 1) soil organic matter inwash, and potentially catchment and lake primary production, and 2) catchment weathering and erosion. Organic content began increasing after 1920 AD to the present, likely in response to warming. Earlier peaks of a similar magnitude occurred on three occasions since 1300 AD, with evidence indicating that these may have coincided with multidecadal-scale periods with higher temperatures, reduced sea ice and negative phases of the North Atlantic Oscillation. Catchment weathering and fluvial erosion began to increase around 1800 AD and peaked during the early 20th century, potentially due to rising temperatures in autumn and winter causing increased liquid water availability. The records suggest that similar levels of erosion and weathering occurred between approximately 1300 and 1600 AD, spanning the transition from the Medieval Climate Anomaly to the Little Ice Age.

Introduction

The Arctic (>60°N) has experienced rapid climate change during the last two centuries, with surface air temperatures increasing by 1.36 °C per century since 1875 AD, which is nearly two times greater than the northern hemisphere trend of 0.79 °C per century (Bekryaev et al. 2010). In agreement with pan-Arctic trends, mean annual air temperatures on Svalbard have increased by ~3-6 °C since 1900 AD, with the strongest temperature increases during the periods 1910-1930 AD and after 1990 AD (Hanssen-Bauer et al. 2019; Isaksen et al. 2022). Sea ice retreat is one of the main factors causing this high latitude warming due to positive feedbacks, including enhanced ocean-atmosphere heat fluxes and a reduced surface albedo, with strong regional warming between 1910 and 1930 AD on Svalbard linked to sea ice moving northwards along the west coast (Hanssen-Bauer and Førland 1998; Isaksson et al. 2003; Divine and Dick 2006). The warming has caused some notable changes on Svalbard, including a 7% reduction of glacier area in the last 30 years (Nuth et al. 2013), an increase in permafrost temperature and active layer depth (Hanssen-Bauer et al. 2019) and ecological changes in both marine and terrestrial food webs (Descamps et al. 2017).

Warming also has a strong impact on Arctic lakes because cryospheric components of the system (such as ice and snow cover) are sensitive to temperature changes, which then strongly influence the physical and biological processes in the lake and catchment. For example, changes in the length of the ice-free season can alter lake productivity, changes in temperature alter lake stratification, and catchment changes in vegetation, glacial activity and weathering can alter the amount of material available for erosion and inwash to lakes (Birks et al. 2004; Rubensdotter and Rosqvist 2009; Holm et al. 2012; de Wet et al. 2018; Woelders et al. 2018). While direct observational records of lake characteristics are short in length, studies of lake sediments have yielded a longer perspective on the nature of recent changes in lakes on Svalbard (Birks et al. 2004; Holmgren et al. 2010; Woelders et al. 2018). Such studies have shown increases in primary production and organic matter during the 20th century, which is hypothesized to be a response to higher temperatures (Birks et al. 2004; Holmgren et al. 2010; Jiang et al. 2011; Woelders et al. 2018), increased nitrogen deposition (Holmgren et al. 2010) and greater inwash of organic material from the catchment due to an increase in precipitation (Birks et al. 2004; Boyle et al. 2004).

Growing concerns about the impact of changes in climate on Svalbard has motivated research to establish a pre-anthropogenic baseline for ecosystem disturbances, to assess whether recent changes exceed natural variability. Furthermore, as palaeoclimate research has indicated that the climate on Svalbard during the last millennium has varied, with multi-centennial climate deviations referred to as the Medieval Climate Anomaly (MCA; c. 900-1350 AD) and the Little Ice Age (LIA; c. 1400-1850 AD) (Divine et al. 2011; D'Andrea et al. 2012; Luoto et al. 2018; van der Bilt et al. 2019; Werner et al. 2018), lake sediment records provide an opportunity to assess the lake and catchment system response to climate perturbations.

In this study, we assess the response of a lake on western Svalbard to climate variability using a geochemical sediment record dating back to c. 1300 AD. Information about past environmental changes in the lake and catchment are obtained by analysing the total organic carbon (TOC) and total nitrogen (TN) content, stable isotope ratios of carbon ($\delta^{13}C$) and nitrogen ($\delta^{15}N$) and elemental composition (X-ray fluorescence; XRF) of two sediment cores, supported by an independent chronology based on lead (^{210}Pb), cesium (^{137}Cs) and accelerator mass spectrometry (AMS) radiocarbon (^{14}C) dating. This allows us to examine the rate and timing of recent changes in lake-catchment-climate interactions.

Study Area

Prins Karls Forland is an 85 km long, 5-11 km wide island west of Spitsbergen, separated from the mainland by the Forlandssundet Strait (Fig. 1a). The studied lake, Blokkvatnet (78°78'N, 10°71'E; 70 m a.s.l.), is located in MacKenziedalen, on the northern part of the island (Fig. 1b). This is a narrow east-west oriented valley situated between two mountain ridges: St. Andreashaugane (541 m a.s.l.) to the south and Stairhøgdene (506 m a.s.l.) to the north (Fig. 1b). The bedrock of the western side of the Blokkvatnet catchment is Tonian slate, meta-sandstone, quartzite and conglomerates, while to the east the bedrock consists of Late Ediacaran carbonates, slates and sandstone, locally covered by blocky till (Dallmann 2015).

Blokkvatnet is a small lake (0.24 km^2) with a maximum water depth of 31 m in the centre. It is ultraoligotrophic, with pH ranging from 7.3-7.5 (measured in August 2009), and it is ice-covered from October to May. The surrounding catchment is sparsely vegetated with mosses and herbs. There are no glaciers in the catchment and therefore no glacial run-off enters the lake, however it receives water from several small streams from the surrounding mountain slopes and has an outlet on the eastern edge (Fig. 1b).

The average temperature of the coldest month (February) and the warmest month (July) at the closest meteorological station (Ny-Ålesund; c. 30 km northeast of the study site) was -11.7 °C and 5.8 °C, respectively, during the period 1993-2011 AD (Maturilli et al. 2013). From 1975-2014 AD, the warming rate at Ny-Ålesund was 0.76 ± 0.29 °C per decade, with stronger warming of 1.04 ± 0.84 °C per decade from 1998-2014 AD (Ding et al. 2018). The mean annual precipitation at Ny-Ålesund was 385 mm from 1961-1990 AD, increasing to a mean of 447 mm in the period 1979-2018 AD (Førland et al. 2011; 2020).

Materials and methods

Field sampling

Two cores were sampled from Blokkvatnet using an Uwitec Corer (diameter 6 cm, tube length 60 cm): a short, 12 cm long core (BV1) was extracted in August 2009 AD at 18 m water depth and a 27.5 cm long core (BV2) was taken in March 2013 AD approximately 150 m northwest of BV1 at 30 m water depth. BV1 was sliced in the field at 0.25 cm resolution and put into sealed plastic bags, while BV2 was wrapped in plastic and stored frozen prior to subsampling. BV2 was subsequently split into two halves and allowed to thaw at room temperature.

Chronology

The chronological constraints available for the two Blokkvatnet cores are twenty-one ^{210}Pb ages from surface sediments measured on the BV1 core between 0 and 5.125 cm (where total ^{210}Pb activity reached equilibrium with ^{226}Ra; Electronic Supplementary Material 1 (ESM1)) and one AMS ^{14}C date from the BV2 core at 20.3 cm (Fig. 2, Table 1). Further radiocarbon dating of both cores was hampered by a lack of terrestrial macrofossils preserved within the core sediments, an issue sometimes encountered in palaeolimnic research on Svalbard (e.g., D'Andrea et al. 2012).

Sediment samples from BV1 were analysed for ^{210}Pb, ^{226}Ra, and ^{137}Cs by direct gamma assay at the Liverpool University Environmental Radioactivity Laboratory, using Ortec HPGe GWL series well-type coaxial low background intrinsic germanium detectors (Appleby et al. 1986). The absolute efficiencies of the detectors were determined using calibrated sources and sediment samples of known activity.

Corrections were made for the effect of self-absorption of low energy γ-rays within the sample (Appleby and Oldfield 1992). The ^{210}Pb dating approach is described in full in ESM1.

Given the limited age constraints on core BV2, a tuning approach was used to transfer the ^{210}Pb dates from core BV1 to BV2 (detailed in ESM2). This was based on variability in the zirconium (Zr) record of each core, which was selected as a conservative element. Eight tie points were used to fit the upper 6 cm of the BV1 Zr record, measured by X-ray fluorescence (XRF) analysis, to the upper 6 cm of the BV2 Zr record, measured using an ITRAX XRF core scanner. This allowed the depths for each ^{210}Pb date to be adjusted accordingly.

One AMS radiocarbon date was obtained from a bryophyte handpicked from core BV2 (20.3 cm depth), which was analysed at the Poznan Radiocarbon Laboratory in Poland. Age-depth models for BV1 and BV2 were developed separately, with the BV1 chronology based on the original ^{210}Pb ages and depths, and the BV2 chronology based on the tuned ^{210}Pb depths and the AMS radiocarbon date. The age-depth models for BV1 and BV2 were produced in R (version 4.1.1.; R Core Team 2020), using the Bayesian Bacon package (version 2.5.7.; Blaauw and Christen 2011). The calibration of the radiocarbon date was based on the IntCal20 calibration curve (Reimer et al. 2020). The median of the modelled 2-sigma age range was used to estimate the down-core calendar year ages.

TOC, TN, C and N isotopes, C:N

Analysis of stable isotopes $\delta^{13}C$ and $\delta^{15}N$ (the ratios of $^{13}C/^{12}C$ and $^{15}N/^{14}N$, respectively), total organic carbon (TOC wt %) and total nitrogen (TN wt %) was conducted on BV1 (48 samples) and BV2 (32 samples) to assess changes in sediment characteristics. On BV1, measurements were made at 0.25 cm contiguous increments throughout the core. TOC, TN, $\delta^{13}C$, and $\delta^{15}N$ were determined by isotope-ratio mass spectrometry ANCA GSL 20-20 (Sercon PDZ Europa) at the Animal and Plant Sciences Research

Laboratory, University of Sheffield. On BV2, these measurements were made at a resolution of 0.5 cm for the top 5 cm and at 1 cm resolution for the remaining core. Samples were freeze-dried and homogenised and then analysed at the Department of Geological Sciences, Stockholm University, using a Carlo Erba NC 2500 elemental analyser (EA) connected to a Finnigan MAT Delta V mass spectrometer. The stable isotope ratios, TOC and TN content were measured simultaneously at a combustion temperature of 1020 °C and with a relative error of less than 1%. The isotopic compositions are expressed as standard delta (δ) notation, with $\delta^{13}C$ samples reported in per mil (‰) relative to international Vienna Pee Dee Belemnite (V-PDB) (Coplen 1995) and $\delta^{15}N$ relative to air. The precision for $\delta^{13}C$ and $\delta^{15}N$ was calculated to be better than 0.15‰, based on the standard deviation from internal standards measured with each run sequence. The TOC and TN measurements were subsequently used to calculate the carbon-to-nitrogen (C:N) atomic ratio through BV1 and BV2 (Meyers 1994; Meyers and Teranes 2001).

X-ray fluorescence (XRF) geochemistry

The geochemical composition of the shorter BV1 core was measured using quantitative XRF analysis, which enabled confirmation of the semi-quantitative XRF analysis approach applied to the longer BV2 core.

The dried bulk sediment of BV1 was measured by energy dispersive X-ray fluorescence analyses (EDXRFA with Spectro –XEPOS) of fine-ground powder in Chemplex-Spectro Micro Cups 3110 at the Institute of Mineralogy and Petrography, University of Innsbruck. The samples were measured at 0.25 cm resolution.

Elemental measurements for BV2 were obtained using an ITRAX XRF core scanner (Croudace et al. 2006) at the Department of Geological Sciences, Stockholm University. Non-destructive element analysis was conducted using a molybdenum (Mo) anode X-ray tube (settings: 30 kV, 45 mA, dwell time 10 seconds) at 200 µm increments along the core. ITRAX core scanners provide semi-quantitative measures of element concentrations by focusing an XRF beam at the sediment surface and then measuring as counts the fluorescent X-rays generated (Croudace et al. 2006). The measured counts can be altered by variations in organic matter, water content and surface roughness, which increase scattering (Croudace et al. 2006; Löwemark et al. 2011). In addition to this, the measured element count can be altered by changes in the concentration of other elements, or organic matter, which are referred to as the 'matrix effect' and 'dilution effect' respectively (e.g., Löwemark et al. 2011). To address these issues the results were normalised using a log-ratio approach (Weltje and Tjallingii 2008; Croudace et al. 2019) with titanium selected as the denominator because it is a conservative element. The results for the section 27.5-25.9 cm on core BV2 were removed due to anomalous measurements by the ITRAX core scanner over this lowermost part of the core. These anomalies were identified by large deviations in the Mean Squared Error and thousand counts per second (kcps) measurements, which are useful indicators of anomalies and artefacts in ITRAX data (Löwemark et al. 2019), and probably the result of a damaged or sloping sediment surface.

Principal Component Analysis

Principal Component Analysis (PCA) was conducted on the results for core BV1 to identify shared patterns of variability in our multi-proxy dataset. The data included in this analysis were the TOC, TN, $\delta^{13}C$ and $\delta^{15}N$ records and the elemental XRF data. As the elemental results are composite data, they are subject to the constant-sum constraint, whereby changes in one variable will lead to changes in others, which can create misleading correlations between variables (Aitchison 1983; Kucera and Malmgren 1998). Therefore prior to PCA analysis, a centred log-ratio transformation of the data was applied (Aitchison 1983; Kucera and Malmgren 1998) using the CoDaPack version 2.02.21 software (Comas-Cufi and Thió-Henestrosa 2011) and the data was standardised. PCA was performed in R using the 'prcomp' function in the Stats package; this performed a singular value decomposition on the data.

Results

Chronology

The calculated age constraints are shown in Table 1 and the age-depth models in Fig. 2, with further information about the original and tuned ^{210}Pb dating results in ESM1 and ESM2. Measurements of ^{137}Cs activity conducted on BV1 samples showed an activity maximum at 1.75-2.5 cm (ESM1), attributed to the 1963 AD peak in atmospheric nuclear bomb testing. This provides independent support for the ^{210}Pb ages, as the ^{210}Pb-based modelled chronology agrees that 1963 AD corresponds to a depth of 2.5 cm in core BV1 (Table 1). The developed chronologies show that the BV1 core spans the period since c. 1700 AD and the BV2 record spans the period since c. 1300 AD (Fig. 2). The ^{210}Pb dating on BV1 (Table 1) shows that sedimentation since c.1870 AD was rather constant between 0.02 and 0.03 g cm^{-2} yr^{-1}, but was higher from c. 1915-1940 AD, with a peak of 0.08 g cm^{-2} yr^{-1} at c. 1926 ± 8 AD.

The developed age-depth models are limited by the lack of age constraints in the lower parts of BV1 and BV2, which has contributed to centennial age uncertainties prior to c. 1850 AD (Fig. 2). The extrapolation of ages for the lower depths of BV1 and BV2 and the interpolation between the ^{210}Pb dates and the ^{14}C date for BV2 also assume that the long-term sedimentation rate in Blokkvatnet was constant, despite variations being likely. Therefore, while the chronologies of both BV1 and BV2 are robust for the period since approximately 1850 AD, there is far less certainty about the modelled ages prior to this, which should be treated with caution.

TOC, TN, C and N isotopes, C:N

The Blokkvatnet sediments (Fig. 2) consist mainly of brownish-grey, finely laminated gyttja silt. In core BV2 there were several darker bands identified at approximately 25 cm (c. 1350 AD), 22.5 cm (c. 1400 AD), 20-18 cm (c. 1450-1500 AD), 16 cm (c. 1580 AD), 15 cm (c. 1600 AD), 14 cm (c. 1650 AD), 10-9 cm (c. 1750 AD) and 8-7 cm (c. 1800 AD). The upper 5 cm (since c. 1900 AD) consisted of homogenous, brown gyttja silt. Furthermore, sandy gyttja silt was identified at depths of 26.8-26.5 cm (c. 1320 AD), 25.6- 25.1 cm (c. 1340 AD), 20.8-19.3 cm (c. 1450-1500 AD) and at 7.2 cm (c. 1830 AD). In the shorter BV1 core the sediment was generally homogenous brown gyttja silt, although there were fine layers of sand and silt identified at 5.75 and 3 cm depths (c. 1860 and 1945 AD respectively) and darker sediments at 11, 7.5 and 6 cm depths (c. 1740, 1800 and 1850 AD respectively). The lake sediments contain little organic matter, as indicated by the low TOC concentrations (in the range of 0.6 to 2.3%) in the Blokkvatnet cores (Fig. 3a).

The BV1 and BV2 records both show increasing concentrations of TOC, TN and $\delta^{15}N$ in the upper core sections, reflecting the period from c. 1920-1930 AD to the present (Fig. 3a-c). However, the records from the two cores differ prior to this, as the BV1 record shows relatively constant TOC and TN between c. 1700 AD and 1930 AD, while BV2 has a peak during the mid-18th century. This suggests that there was spatially heterogeneous organic deposition within the lake at this time. It is notable that the magnitude of $\delta^{15}N$ changes is also greater in BV1 than BV2, which may be a result of these analyses being conducted in different laboratories using different equipment. During earlier centuries (covered by only core BV2) the TOC, TN and $\delta^{15}N$ show similar patterns of variability, with peaks occurring during the 15th and 17th centuries. The peaks in TOC, TN and $\delta^{15}N$ occur at the same depths as some of the identified dark sediment layers in BV2.

The two $\delta^{13}C$ records (Fig. 3d) both have a large magnitude peak centred at c. 1920-1930 AD ($\delta^{13}C$ of -23 to -22‰) followed by a decline to minimum values in the early 21st century (-26 to -25‰). The high resolution BV1 record has earlier peaks at c. 1870 AD and c. 1750 AD, while the longer and lower-resolution BV2 record has low magnitude peaks during the 14th century and second half of the 16th century.

The BV1 and BV2 C:N records (Fig. 3e) show relatively low values of 6-7 during the 17th to early 20th centuries, with higher values of ~8-10 between c. 1910 and 1960 AD, after which both records indicate a C:N of ~7. The C:N through the longer BV2 record varies between 7 and 8, with a minima at c. 1400 AD and maxima in the 15th and 16th centuries, which is followed by a decreasing trend to the minima in the early 20th century.

XRF geochemistry

The BV1 lake sediments are dominated by SiO_2 (average 59%), with high amounts of Al_2O_3 (average 14%) and Fe_2O_3 (9%), while K_2O (3%), MgO (2%), Na_2O (1%), TiO_2 (0.8%) and CaO (0.7%) account for less than 4% in all layers. The records for a selection of key elements analysed on BV1 and BV2 are shown in Fig. 4, with all the measured element records for the BV1 and BV2 cores presented in ESM3. Comparison of the BV1 XRF results with the normalised BV2 ITRAX XRF results highlights that there are similar patterns of variability between the two cores for some elements (Ca, Fe, Zr, Zn, Sr and Rb), but there are differences between the BV1 and BV2 records for K and Si (Fig. 4). This comparison supports that the normalisation using a log-ratio approach has effectively removed the dilution and matrix effects for many of the BV2 element records measured with the ITRAX core scanner. The inaccurate measurement of K and Si is likely the result of the low atomic numbers of these elements, which Gregory et al. (2019) identified as a factor causing poor detection by XRF cores scanners due to “noise” from matrix and specimen effects. The BV2 K and Si records should therefore be treated with caution and are not considered in the following results or discussion.

The geochemistry results from the BV1 and BV2 cores show some shared patterns of variability between the considered elements since c. 1700 AD. Ca, Fe, Pb, Zn and Rb (Fig. 4) as well as S, As, Ni, Co and Cr (ESM3) peak during the second half of the 18th century, decrease to a minimum c. 1900 AD and increase thereafter. Sr and Rb (Fig.4), as well as Cu, Si, Ca, Zn, Na and Cl (ESM3) also have a peak during the late 18th century but reach a minimum earlier at c. 1850 AD, followed by a gradual increase towards the present. Ti, K, Al, Zr (Fig. 4) and Mg (ESM3), have a minor peak during the late 18th century, lower values during the early 19th century, an increase to a broad maximum at c. 1900 AD, followed by a decrease towards the present.

The longer BV2 record, while limited by poor chronological constraints, shows the long-term range of variability of selected elements during the last millennium (Fig. 4). The results indicate that Ca, Fe, Zn and Sr have peaks or higher values during the 15th and 17th centuries. The Zr record has high variability between c. 1400 and 1600 AD followed by lower variability from c. 1600 to 1850 AD. The Rb record shows low variability, however there is an increasing trend since c. 1700 AD.

Principal Component Analysis

PCA on the elemental and organic parameters for core BV1 shows that the first eigenvector (Principal Component 1; PC1) explains 31% of the variance and the second eigenvector (PC2) explains 25% of the variance (Fig. 5a). Many of the variables have strong loadings on both PC1 and PC2: PC1 has positive loadings for $\delta^{15}N$, TN, TOC, Fe, S, As, Ni, Mn and Pb and negative loadings for Zr, Al, $\delta^{13}C$, K, Rb, Mn, Ti and Zn, while PC2 has positive loadings for $\delta^{15}N$, TN, TOC, Ti, Zn, Si, Na, Cu, Ca, Pb, Fe and Mn, and negative loadings for Co, P, Cr, Mn and Ni (Fig. 5a; Table 2). The eigenvector loadings for PC1 over time show a long-term, gradual decrease from the early 18th century to c. 1920 AD, followed by increasingly positive loadings from 1920 AD to the present (Fig. 5b). The eigenvector loadings over time for PC2 feature increasingly positive loadings from c. 1800 AD onwards (Fig. 5b).

Discussion

Here we use the multiple proxies from analysis of the two sediment cores from Blokkvatnet and compare them to observational and palaeoclimate records available from Svalbard, to understand the sources and variability of mineral and organic matter deposition in the lake.

Organic matter deposition

Discussion of proxies associated with organic matter deposition

The core BV1 proxies with positive PC1 loadings (including TOC, TN, $\delta^{15}N$, Fe, Pb, Mn, Ni, S, As; Table 2) have higher values at c. 1800 AD, a drop at 1920 AD and increase thereafter, although the higher values at 1800 AD are not shown by the BV1 TOC and TN records (Figs. 3, 4, 5; ESM3). Similar trends are shown by the BV2 core in the variability of Fe, TOC, TN and $\delta^{15}N$ (Figs. 3, 4), although fewer elements were measured on BV2 and Mn shows contrasting patterns of variability (ESM3).

The simultaneous changes in the organic parameters (particularly TOC) and elemental variables (especially Fe, Pb, Ni, S, As) may be interpreted in a number of ways. The inwash of soil organic matter to Blokkvatnet is a likely source of organic matter. Previous research on Svalbard concluded that inwashed soil organic matter caused changes in organic content, based on the simultaneous increases in organic matter and Pb within lake sediments, as the concentration of Pb would be diluted and decrease if the organic matter was autochthonous in origin (Boyle et al. 2004). The results from Blokkvatnet support a similar interpretation, as the concentration of several elements including Pb increase in the layers of BV1 that have higher TOC (Fig. 3, 4).

However, as TOC can be altered by a combination of within-lake production, decomposition, redox related diagenetic processes, as well as the amount of inwashed soil organic matter, other contributions to the variations in organic content cannot be excluded. A previous study has shown that in Arctic lakes TOC varies in phase with chlorophyll concentrations, supporting that organic deposition can reflect changes in primary production (Michelutti et al. 2005). Indeed, the BV1 and BV2 C:N records show a small decrease in the late 20th century, which supports that there may have been an enhanced contribution of organic matter from within-lake sources (Meyers and Teranes 2001). The co-variance between the $\delta^{15}N$ and TOC may also support that the TOC peaks were caused by greater algal production; phytoplankton favour ^{14}N over ^{15}N, therefore when algal production increases and ^{14}N in surface water diminishes, phytoplankton use more ^{15}N rather than ^{14}N, resulting in ^{15}N enrichment in the sediment and higher $\delta^{15}N$ values (Hodell and Schelske 1998). Previous research on Arctic lakes has shown a coupling between proxies for primary production (e.g., $BSiO_2$ and loss-on-ignition) and $\delta^{15}N$ (Hu et al. 2001; Wolfe et al. 2006). However, as the $\delta^{15}N$ signature of sediment can also be influenced by changes in N source and internal microbial cycling, the interpretation of this proxy is uncertain (Botrel et al. 2014). A more in-depth assessment of the link between changes in TOC and primary production in Blokkvatnet using diatom concentrations is prevented by the poor preservation of diatom valves in the sediment.

The co-variability between certain elements and TOC along BV1 may also reflect the affinity of heavy metals (including Pb, Cu, Ni, Co, Zn, Ca, Fe, Mn and Mg) to bind to organic matter within soils, as well as within the waters and sediments of lakes (Horowitz 1991). The changes in the deposition of organic matter therefore may have enhanced the concentration of some of these elements within the sediments when TOC increased, regardless of the organic matter source.

Climate influence on organic deposition

Temperatures on Svalbard increased rapidly between 1910 and 1920 AD leading to a period of relative warmth during the early 20th century from 1920-1950 AD, which was particularly pronounced during autumn and winter months (Fig. 5c). This has been linked with stronger westerly winds, enhanced oceanic heat transport and a northward retreat of sea ice from the coast of Svalbard (Hanssen-Bauer and Førland 1998; Isaksson et al. 2003; Bengtsson et al. 2004; Divine and Dick 2006; Woelders et al. 2018; Norwegian Meteorological Institute 2022). The strong winds and reduced sea ice may explain the elevated levels of elements associated with sea spray at this time, shown by peaks in Cl (BV1) and Br (BV2; ESM3). PC1 had negative loadings at this time, which likely reflects the enhanced deposition of inorganic sediments at c.1915-1940 AD causing dilution of the organic matter (and variables with PC1 positive loadings) within the sediments, as discussed in the following section.

The warming during all seasons through the twentieth century may have caused the changes captured by increasingly positive loadings of PC1 after c. 1920 AD (Fig. 5c; Norwegian Meteorological Institute 2022). We speculate that there may have been an increase of inwashed soil connected to increased exposure each summer of the soil surface, as a result of diminishing snow cover with warming. This is supported by evidence that since 1961 AD the minimum snow cover on Svalbard at the end of summer has decreased from 48% to 36%, potentially causing a greater snow-free area within the Blokkvatnet catchment, and the snow-free season length has increased by 1.2 days per decade (van Pelt et al. 2016). However, primary production within the lake may have also increased, as indicated by the lower C:N after 1960 AD (Fig. 3e). An increase in organic matter accumulation rates and abundances of diatom valves and chrysophyte cysts in lakes elsewhere on Svalbard during the last 50-100 years supports that there has been increasing levels of primary production within some lakes (Holmgren et al. 2010; Jiang et al. 2011; Woelders et al. 2018).

An alternative explanation for the variability in TOC and associated elements may be that past changes in bird populations in the catchment caused the simultaneous deposition of elements found in bird faeces (including Fe, Mn, Ni, Pb; Kozak et al. 2015), as well as enhanced organic deposition, as additional nutrients may have stimulated enhanced plant growth in the catchment (Yang et al. 2021) and productivity within the lake (Luoto et al. 2014). The available evidence however does not support this hypothesis, because the dominant bird populations on Prins Karls Forland (the Little Auk and Brunnichs Guillemot; Kempf and Sittler 1988), appear to have been negatively affected by warming over recent years and decades (Hovinen et al. 2014; Fauchald et al. 2015) and typically nest on coastal cliffs rather than around lakes.

During the last millennium, periods with greater deposition of organic sediment may have coincided with intervals of higher temperatures and sea ice retreat to the west of Svalbard, resembling changes during the 20th century (Fig. 6), although the chronological limitations of the BV2 core mean that these climate-environment interactions are speculative.

Analysis of an ice core from Holtedahlfonna, located to the northeast of Ny-Ålesund (Fig. 1a), shows that around 1750 AD there were elevated levels of sea-spray ions (Cl, Na, K, Mg) and a peak in methanesulfonic acid, a proxy for marine productivity and sea-ice cover (Isaksson et al. 2005; Beaudon et al. 2013), supporting the conclusion that the sea ice had retreated. An ice core $\delta^{18}O$ record from Austfonna (Fig. 1a) shows a decade with prolonged warmth from 1740-1750 AD (Isaksson et al. 2003; Fig. 6d). As in the 20th century, these changes may coincide with changes in the Blokkvatnet records, including the onset of enhanced organic deposition (shown by TOC in core BV2; Fig. 6b), peaks in some elements (including Ca, Sr, Zn, Rb in both BV1 and BV2, and Pb, S and As in BV1; Fig. 4, ESM3) and deposition of marine aerosols (Cl and Na in BV1; ESM3). Similar warmer intervals may have also occurred during the 15th and 16th centuries; the core BV2 records suggest that at these times there were peaks in organic content that appear to have been initiated by warmer climate intervals ($\delta^{18}O$ peaks in the Austfonna record; Fig. 6d).

The deposition of the organic layers in Blokkvatnet and higher temperatures on Svalbard (Isaksson et al. 2003) could have resulted from atmospheric circulation associated with the negative phase of the North Atlantic Oscillation (NAO) index (Fig. 6). Negative NAO circulation patterns are associated with higher temperatures and reduced precipitation in winter on Svalbard (Osuch and Wawrzyniak 2017). Although the BV1 and BV2 records have significant chronological uncertainties, there appears to be similar timings for reconstructed negative NAO excursions (Trouet et al. 2009; Fig. 6c) and intervals of slightly increased organic deposition in Blokkvatnet of ~1% (Fig. 6b), supporting a consistent relationship between temperature and organic sediment deposition during the last millennium.

When placed in a long-term context, the BV2 record shows that the changes that have occurred in Blokkvatnet and the surrounding catchment during the 20th century are not unusual in magnitude compared to changes since 1300 AD. However, the higher-resolution BV1 record shows more muted variability during the last 300 years and therefore the increase in organic matter deposition during the 20th century was significantly above previous levels (Fig. 3a). While it appears that natural climate variability has influenced the deposition and production of organic matter within the lake during the last ~700 years, albeit with some spatial heterogeneity, the results support that anthropogenic warming during the 20th century has also had a strong influence on the Blokkvatnet lake and catchment. It is therefore likely that continued warming will cause organic matter deposition exceeding the range of natural variability.

Catchment weathering and erosion

Discussion of proxies associated with weathering and erosion

Several of the BV1 records with negative loadings for PC1 show a peak at c. 1920 AD (including $\delta^{13}C$, Zr, Al, Mg, K and Ti), which is also captured by the Rb/Sr and C:N records not included in the PCA analysis (Figs. 3, 4). A similar peak is observed in the BV2 records for $\delta^{13}C$, C:N and Zr (Fig. 4). A selection of these records has been standardised and presented in Fig. 7 to aid comparison.

We hypothesise that these variables reflect catchment weathering and erosion, as well as inwash to Blokkvatnet. This interpretation is based on the conservative and geologically abundant nature of the elements that peak at c. 1920 AD, which supports that they reflect catchment inwash of weathered and eroded minerogenic material. For example, conservative element Zr is an insoluble mineral considered to be a sensitive proxy for physical erosion (Wolfe and Hätling 1997). Rb/Sr may provide a proxy for weathering; Sr is leached more easily than Rb from rocks, therefore strong chemical weathering will result in sedimentation with low Rb/Sr, whereas physical weathering, such as freeze-thaw, will cause sedimentation with higher Rb/Sr values (Xu et al. 2010). The variability in Rb/Sr however may also reflect changes in the grain size of inwashed sediments; fine sediments have a greater surface area, therefore Sr is leached more rapidly than in coarse grains, resulting in fine (coarse) sediments having higher (lower) Rb/Sr ratios (Alexandrin et al. 2018). The C:N ratio can reflect changes in the origin of organic material as higher values (>20) can be caused by allochthonous sources (Meyers and Terranes 2001). Finally, while a number of different factors can influence the $\delta^{13}C$ of lake sediments, including changes in lake productivity (Briner et al. 2006; Jiang et al. 2011), the similar timing of peaks in $\delta^{13}C$ with higher C:N suggests that it may be reflecting variations in the inwash of plant or soil organic matter with a less negative isotopic signature. However, this is speculative because Svalbard has C3 plants rather than C4 plants (Collins and Jones 1986), and C3 plants have a $\delta^{13}C$ signature that is indistinguishable from lake algae (Meyers 1994).

The interpretation that the interval c. 1920 AD was a period with enhanced catchment erosion and weathering is supported by the high sedimentation rate between 1915 and 1940 AD detected by the ^{210}Pb dating (Table 1; ESM1). The enhanced influx of material may have diluted the organic matter being deposited within the lake, partly contributing to the reduction in TOC and elements with positive PC1 loadings discussed previously.

Climate influence on catchment weathering, erosion and inwash

Climatic factors may have altered the amount of erosion and weathering in the Blokkvatnet catchment and the inwash of material to the lake. Although there are only fragmented meteorological data for Svalbard prior to the 20th century (Przybylak et al. 2016), it is known that there were lower temperatures between 1900 and 1915 AD and a warmer period between 1920 and 1950 AD, with warming most pronounced during autumn and winter (Hanssen-Bauer et al. 2019; Norwegian Meteorological Institute 2022; Fig. 5c). The higher temperatures in the early 20th century may have caused enhanced inwash to Blokkvatnet, due to more frequent rainfall and greater snow and ice melt during the autumn and winter months. We also speculate that enhanced physical weathering may have occurred as indicated by the peak in Rb/Sr at this time in core BV1; freeze-thaw weathering in cold regions is often water limited (Hall et al. 2002), therefore an increase in rainfall and/or snow melt events during the autumn and winter may have enhanced this process. Temperatures between c. 1960 and 1995 AD were 1-2°C cooler than between c. 1920 and 1960 AD (Hanssen-Bauer et al. 2019; Fig. 5c), and this may have reduced the catchment erosion and weathering of sediment during these decades, as indicated by a reduction in the considered variables in both cores (Fig. 7).

During the last millennium, although there is high chronological uncertainty for the early BV2 record (Fig. 7c), the multi-centennial changes in Zr and C:N (Fig. 6b) suggest the inwash of catchment mineral and organic material was lower between c. 1600 and 1850 AD, during the latter part of the LIA, and higher at c. 1300 to 1600 AD during the final phase of the MCA and transition into the LIA. This appears to indicate that the higher temperatures prior to 1600 AD, as suggested by some but not all records (Divine et al. 2011; D'Andrea et al. 2012; Luoto et al. 2018; Werner et al. 2018; van der Bilt et al. 2019), caused changes in erosion of similar magnitude to those during the early 20th century.

The second Principal Component for BV1 shows a long-term trend towards increasingly positive loadings from 1800 AD to the present (Fig. 5). This reflects increasing trends of variables, in particular Rb, Zn, Pb, Ca, Cl, TOC and TN and to a lesser extent Si, Ti, Cu, since 1800 AD, and negative trends in P and Mn (Fig. 5; ESM3; Table 2). A synchronous increase is also observed in the BV1 C:N record (Fig. 3) and Rb/Sr record (Fig. 4), which were not included in the PCA. In line with the proxy interpretations discussed previously, the results may indicate that there was a gradual increase in physical weathering of catchment rocks (Rb/Sr) and inwash of organic matter (C:N), thus causing an increased deposition of elements derived from catchment rocks and soil. While instrumental records are not available for the period prior to the twentieth century, the Austfonna $\delta^{18}O$ record (Fig. 6c) suggests that there was a steady rise in temperature after 1800 AD on Svalbard (Isaksson et al. 2003) reflecting wider Arctic warming trends (Kaufman et al. 2009), which may have caused these changes in sediment deposition from the Blokkvatnet catchment. This interpretation is similar to that for the variables with negative PC1 loadings, however the individual signatures of the two principal components suggest that they are related to different processes and/or different rock and soil types.

Conclusions

We employed a multi-proxy approach to reconstruct recent and past environmental changes in lake Blokkvatnet, Svalbard, since c. 1300 AD, to assess how climate changes have affected the lake. Elemental analysis (using traditional XRF and ITRAX XRF core scanning) and stable isotope analysis (TOC, $\delta^{13}C$, TN, $\delta^{15}N$, C:N) were applied to two sediment cores. Three groups of proxies were identified using Principal Component Analysis (PCA). We suggest that these primarily reflect different sources of catchment inwash to Blokkvatnet occurring during different seasons.

The first group had positive loadings for PC1, with shared variability between TOC, $\delta^{15}N$, TN and elements including Pb, Fe, S, As and Ni, and may reflect the inwash of soil organic matter. These proxies gradually increased after 1920 AD, therefore we hypothesise that increasing temperatures during the 20th century reduced the duration of snow cover, leading to an increase in soil exposure and inwash to Blokkvatnet. Warming may have also potentially caused greater within-lake primary production. Three earlier peaks in TOC during the 15th, 17th and 18th centuries were of similar magnitude to the 20th

century increase in organic matter. Although the early part of the record lacks strong chronological constraints, we tentatively associate these peaks with periods that had higher temperatures on Svalbard, potentially forced by negative NAO circulation patterns and reduced sea ice.

The second identified group had negative loadings for PC1 with shared variability between Rb/Sr, C:N, $\delta^{13}C$ and elements including Zr, Al, Mg, K and Ti, and may reflect the erosion, weathering and inwash from the catchment to Blokkvatnet. These proxies peaked between 1900 and 1950 AD during a period when temperatures increased on Svalbard, particularly during autumn and winter, which we suggest may have caused greater frequency of snowmelt and rainfall events, leading to enhanced freeze-thaw weathering and erosion. During the last millennium, peaks in Zr and C:N values were of similar magnitude to the 20th century prior to c. 1600 AD, indicating weathering and erosion were also enhanced during the late MCA and early LIA.

Finally, PC2 captured an increasing trend since 1800 AD in some elements (particularly Rb, Zn, Pb, Ca), as well as Rb/Sr and C:N, that coincided with a multi-centennial warming trend on Svalbard, suggesting that long-term warming may have enhanced the catchment weathering and erosion over recent centuries.

Acknowledgements

We would like to thank Jakub Zarsky and Michelle Harlton Maccrackin for fieldwork assistance in 2009, Henrik Rasmussen for field assistance in 2013 and the Svalbard Science Forum and Norwegian Polar Institute for supporting the fieldwork. Stefan Wastegård is thanked for laboratory assistance. Thanks to Richard Tessadri, University of Innsbruck, for XRFA measurements of BV1, and to P.G.Appleby and

G.T.Piliposyan, University of Liverpool, for ^{210}Pb and ^{137}Cs dating. We thank the NSINK group, esp. Andy Hodson, for helpful discussions during meetings. This work was supported within the Marie Curie Initial Training Network NSINK ITN-2007.1.1, ENV. 215503 and The Research Council of Norway project 193902/V11. KK received support by the Melting Project of the Austrian Academy of Sciences (ÖAW grant to KK) and by the Nickel Control Project of the Autonomous Province Bolzano/Bozen (grant to KK).

References

Aitchison J (1983) Principal component analysis of compositional data. Biometrika 70(1): 57-65. https://doi.org/10.1093/biomet/70.1.57

Alexandrin MY, Darin AV, Kalugin IA, Dolgova EA, Grachev AM, Solomina ON (2018) Annual sedimentary record from Lake Donguz-Orun (Central Caucasus) constrained by high resolution SR-XRF analysis and its potential for climate reconstructions. Front Earth Sci 6: 158. https://doi.org/10.3389/feart.2018.00158

Appleby PG, Nolan PJ, Gifford DW, Godfrey MJ, Oldfield F, Anderson NJ, Battarbee RW (1986) 210Pb dating by low background gamma counting. Hydrobiologia 143(1): 21–27. https://doi.org/10.1007/BF00026640

Appleby PG, Oldfield F (1992) Applications of lead-210 to sedimentation studies. In Uranium-series disequilibrium: applications to earth, marine, and environmental sciences. 2. ed. United Kingdom: Clarendon Press.

Beaudon E, Moore JC, Pohjola VA, Van de Wal RSW, Kohler J, Isaksson E (2013) Lomonosovfonna and Holtedahlfonna ice cores reveal east – west disparities of the Spitsbergen environment since AD 1700. J Glaciol 59(218): 1069–1083. https://doi.org/10.3189/2013JoG12J203

Bekryaev RV, Polyakov IV, Alexeev VA (2010) Role of polar amplification in long-term surface air temperature variations and modern Arctic warming. J Clim 23(14): 3888–3906.https://doi.org/10.1175/2010JCLI3297.1

Bengtsson L, Semenov VA, Johannessen OM (2004) The early twentieth-century warming in the Arctic—A possible mechanism. J Clim 17(20): 4045-4057. https://doi.org/10.1175/1520-0442(2004)017%3C4045:TETWIT%3E2.0.CO;2

Birks HJB, Jones VJ, Rose NL (2004) Recent environmental change and atmospheric contamination on Svalbard as recorded in lake sediments – synthesis and general conclusions. J Paleolimnol 31: 531–546. https://doi.org/10.1023/B:JOPL.0000022550.81129.1a

Blaauw M, Christen JA (2011) Flexible paleoclimate age-depth models using an autoregressive gamma process. Bayesian Anal 6(3): 457–474. https://doi.org/10.1214/11-BA618

Botrel M, Gregory-Eaves I, Maranger R (2014) Defining drivers of nitrogen stable isotopes (δ 15 N) of surface sediments in temperate lakes. J Paleolimnol 52(4): 419-433. https://doi.org/10.1007/s10933-014-9802-6

Boyle JF, Rose NL, Appleby PG, Birks HJB (2004) Recent environmental change and human impact on Svalbard : the lake-sediment geochemical record. J Paleolimnol 31: 515–530. https://doi.org/10.1023/B:JOPL.0000022549.07298.6e

Briner JP, Michelutti N, Francis DR, Miller GH, Axford Y, Wooller MJ, Wolfe AP (2006) A multi-proxy lacustrine record of Holocene climate change on northeastern Baffin Island, Arctic Canada. Quat Res 65: 431–442. https://doi.org/10.1016/j.yqres.2005.10.005

Collins RP, Jones MB (1986) The influence of climatic factors on the distribution of C4 species in Europe. Vegetatio, 64(2–3), 121–129. https://doi.org/10.1007/BF00044788

Comas-Cufí M, Thió-Henestrosa S (2011) CoDaPack 2.0: a stand-alone, multi-platform compositional software. In: Egozcue JJ, Tolosana-Delgado R, Ortego MI, eds. CoDaWork'11: 4th International Workshop on Compositional Data Analysis. Sant Feliu de Guíxols; 2011.

Coplen TB (1995) Reporting of stable hydrogen, carbon, and oxygen isotopic abundances. Geothermics, 5(24), 707–712. https://doi.org/10.1016/0375-6505(95)00024-0

Croudace IW, Rindby A, Rothwell RG (2006) ITRAX: description and evaluation of a new multi-function X-ray core scanner. Geological Society, London, Special Publications, 267(1), 51–63.

Croudace IW, Löwemark L, Tjallingii R, Zolitschka B (2019) Current perspectives on the capabilities of high resolution XRF core scanners. Quat Int 514: 5-15. https://doi.org/10.1016/j.quaint.2019.04.002

Dallmann WKE (2015) Geoscience Atlas of Svalbard. Norwegian Polar Institute, Report Series 148, 292 pp

D’Andrea WJD, Vaillencourt DA, Balascio NL, Werner A, Roof SR, Retelle M, Bradley RS (2012) Mild Little Ice Age and unprecedented recent warmth in an 1800 year lake sediment record from Svalbard. Geology 40 (11): 1007–1010. https://doi.org/10.1130/G33365.1

de Wet GA, Balascio NL, Andrea WJD, Bakke J, Bradley RS, Perren B (2018) Holocene glacier activity reconstructed from proglacial lake Gjøavatnet on Amsterdamøya , NW Svalbard. Quat Sci Rev 183: 188–203. https://doi.org/10.1016/j.quascirev.2017.03.018

Descamps S, Aars J, Fuglei E, Kovacs KM, Lydersen C, Pavlova O, Pedersen AØ, Ravolainen V, Strøm H (2017) Climate change impacts on wildlife in a High Arctic archipelago – Svalbard , Norway. Glob Chang Biol 23 (2): 490–502. https://doi.org/10.1111/gcb.13381

Ding M, Wang S, Sun W (2018) Decadal climate change in Ny-Ålesund, Svalbard, a representative area of the Arctic. Condens Matter 3(2): 12. https://doi.org/10.3390/condmat3020012

Divine D, Isaksson E, Martma T, Meijer HAJ, Moore J, Pohjola V, van de Wal RSW, Godtliebsen F (2011) Thousand years of winter surface air temperature variations in Svalbard and northern Norway reconstructed from ice-core data Svalbard and northern Norway reconstructed from ice-core data. Polar Res 30 (1): 7379. https://doi.org/10.3402/polar.v30i0.7379

Divine DV, Dick C (2006) Historical variability of sea ice edge position in the Nordic Seas. J Geophys Res 111: 1–14. https://doi.org/10.1029/2004JC002851

Fauchald P, Anker-Nilssen T, Barrett R, Bustnes JO, Bårdsen BJ, Christensen-Dalsgaard S, Descamps S, Engen S, Erikstad KE, Hanssen SA, Lorentsen SH (2015) The status and trends of seabirds breeding in Norway and Svalbard. NINA report 1151. 84 pp.

Førland EJ, Benestad R, Hanssen-bauer I, Haugen JE, Skaugen TE (2011) Temperature and Precipitation Development at Svalbard 1900 – 2100. Adv Meteorol 893790: 1-14 https://doi.org/10.1155/2011/893790

Førland EJ, Isaksen K, Lutz J, Hanssen-Bauer I, Schuler TV, Dobler A, Gjelten HM, Vikhamar-Schuler D (2020) Measured and Modeled Historical Precipitation Trends for Svalbard. J Hydrometeorol 21(6): 1279–1296. https://doi.org/10.1175/JHM-D-19-0252.1

Hall K, Thorn CE, Matsuoka N, Prick A (2002) Weathering in cold regions: some thoughts and perspectives. Prog Phys Geogr 26(4): 577–603. https://doi.org/10.1191%2F0309133302pp353ra

Hanssen-Bauer I, Førland EJ (1998) Long-Term Trends in Precipitation and Temperature in the Norwegian Arctic: Can They Be Explained by Changes in Atmospheric Circulation Patterns? Clim Res, 10: 143–153. https://doi.org/10.3354/cr010143

Hanssen-Bauer I, Førland EJ, Hisdal H, Mayer S, Sandø AB, Sorteberg A (2019) Climate in Svalbard 2100 - a knowledge base for climate adaptation. Norwegian Centre for Climate Services.

Hodell DA, Schelske CL (1998) Production, sedimentation, and isotopic composition of organic matter in Lake Ontario. Limnol Oceanogr 43(2): 200–214. https://doi.org/10.4319/lo.1998.43.2.0200

Holm TM, Koinig KA, Andersen T, Donali E, Klaveness D (2012) Rapid physicochemical changes in the high Arctic Lake Kongressvatn caused by recent climate change. Aquat Sci 74(3): 385–395. https://doi.org/10.1007/s00027-011-0229-0

Holmgren SU, Bigler C, Ingólfsson Ó, Wolfe AP (2010) The Holocene – Anthropocene transition in lakes of western Spitsbergen, Svalbard (Norwegian High Arctic): climate change and nitrogen deposition. J Paleolimnol 43: 393–412. https://doi.org/10.1007/s10933-009-9338-3

Horowitz AJ (1991) A primer on sediment-trace element chemistry. Chelsea: Lewis Publishers.

Hovinen JE, Wojczulanis-Jakubas K, Jakubas D, Hop H, Berge J, Kidawa D, Karnovsky NJ, Steen H (2014) Fledging success of little auks in the high Arctic: do provisioning rates and the quality of foraging grounds matter?. Polar Biol 37(5): 665-674. https://doi.org/10.1007/s00300-014-1466-1

Hu FS, Finney BP, Brubaker LB (2001) Effects of Holocene Alnus expansion on aquatic productivity, nitrogen cycling, and soil development in southwestern Alaska. Ecosystems 4: 358–368. https://doi.org/10.1007/s10021-001-0017-0

Isaksen K, Nordli Ø, Ivanov B, Køltzow MA, Aaboe S, Gjelten HM, Mezghani A, Eastwood S, Førland E, Benestad RE, Hanssen-Bauer I (2022) Exceptional warming over the Barents area. Sci reports 12(1): 1-8. https://doi.org/10.1038/s41598-022-13568-5

Isaksson E, Hermanson M, Hicks S, Igarashi M, Kamiyama K, Moore J, Motoyama H, Muir D, Pohjola V, Vaikmäe R, van de Wal RSW, Watanabe O (2003) Ice cores from Svalbard — useful archives of past climate and pollution history. Phys Chem Earth 28: 1217–1228. https://doi.org/10.1016/j.pce.2003.08.053

Isaksson E, Kekonen T, Moore J, Mulvaney R (2005) The methanesulfonic acid (MSA) record in a Svalbard ice core. Ann Glaciol 42: 345-351. https://doi.org/10.3189/172756405781812637

Jiang S, Liu X, Sun J, Yuan L, Sun L, Wang Y (2011) A multi-proxy sediment record of late Holocene and recent climate change from a lake near Ny-Ålesund, Svalbard. Boreas, 40(3): 468–480. https://doi.org/10.1111/j.1502-3885.2010.00198.x

Kempf C, Sittler B (1988) Census of breeding seabirds on the northwest coast of Svalbard 1973 and 1978. Polar Res 6(2):195-203. https://doi.org/10.1111/j.1751-8369.1988.tb00598.x

Kozak K, Kozioł K, Luks B, Chmiel S, Ruman M, Marć M, Namieśnik J, Polkowska Ż (2015) The role of atmospheric precipitation in introducing contaminants to the surface waters of the Fuglebekken catchment, Spitsbergen. Polar Res 34(1): 24207. https://doi.org/10.3402/polar.v34.24207

Kucera M, Malmgren BA (1998) Logratio transformation of compositional data: a resolution of the constant sum constraint. Mar Micropaleontol 34(1-2): 117-120. https://doi.org/10.1016/S0377-8398(97)00047-9

Kaufman DS, Schneider DP, McKay NP, Ammann CM, Bradley RS, Briffa KR, Miller GH, Otto-Bliesner BL, Overpeck JT, Vinther BM, Arctic Lakes 2k Project Members (2011) Recent warming reverses long-term Arctic cooling. Sci 325(5945): 1236-1239. https://doi.org/10.1126/science.1173983

Löwemark L, Chen HF, Yang TN, Kylander M, Yu EF, Hsu YW, Lee TQ, Song SR, Jarvis S (2011) Normalizing XRF-scanner data: a cautionary note on the interpretation of high-resolution records from organic-rich lakes. J Asian Earth Sci 40(6): 1250-1256. https://doi.org/10.1016/j.jseaes.2010.06.002

Löwemark L, Bloemsma M, Croudace I, Daly JS, Edwards RJ, Francus P, Galloway JM, Gregory BR, Huang JJ, Jones AF, Kylander M (2019) Practical guidelines and recent advances in the Itrax XRF core-scanning procedure. Quat Int 514: 16-29.

Luoto TP, Brooks SJ, Salonen VP (2014) Ecological responses to climate change in a bird-impacted High Arctic pond (Nordaustlandet, Svalbard). J Paleolimnol 51(1): 87-97. https://doi.org/10.1007/s10933-013-9757-z

Luoto TP, Ojala AEK, Arppe L, Brooks SJ, Kurki E, Oksman M, Wooller MJ, Zajaczkowski M (2018) Synchronized proxy-based temperature reconstructions reveal mid- to late Holocene climate oscillations in High Arctic Svalbard. J Quat Sci, 33: 93–99. https://doi.org/10.1002/jqs.3001

Maturilli M, Herber A, König-Langlo G (2013) Climatology and Time Series of Surface Meteorology in Ny¬Ålesund, Svalbard. Earth Syst Sci Data, 5: 155–163. https://doi.org/10.5194/essd-5-155-2013

Meyers PA (1994) Preservation of elemental and isotopic source identification of sedimentary organic matter. Chem Geol, 114(3–4): 289–302. https://doi.org/10.1016/0009-2541(94)90059-0

Meyers PA, Teranes JL (2001) Sediment Organic Matter. In W. M. Last & J. P. Smol (Eds.), Tracking Environmental Change Using Lake Sediments. Volume 2: Physical and Geochemical Methods. Dordrecht, The Netherlands: Kluwer Academic Publishers.

Michelutti N, Wolfe AP, Vinebrooke RD, Rivard B, Briner JP (2005) Recent primary production increases in arctic lakes. Geophys. Res. Letters 32: 3–6. https://doi.org/10.1029/2005GL023693

Norwegian Meteorological Institute (2018). Air temperature in Svalbard, annual mean. Environmental monitoring of Svalbard and Jan Mayen (MOSJ). URL: http://www.mosj.no/en/climate/atmosphere/temperature-precipitation.html

Norwegian Meteorological Institute (2022). Seasonal temperatures for Svalbard Airport. Environmental monitoring of Svalbard and Jan Mayen (MOSJ). URL: http://www.mosj.no/en/climate/atmosphere/temperature-precipitation.html

Nuth C, Kohler J, König M, von Deschwanden A, Hagen JOM, Kääb A, Moholdt G, Pettersson R (2013) Decadal changes from a multi-temporal glacier inventory of Svalbard. The Cryosphere, 7(5): 1603–1621. http://doi.org/10.5194/tc-7-1603-2013

Osuch M, Wawrzyniak T (2017) Inter-and intra-annual changes in air temperature and precipitation in western Spitsbergen. Int J Climatol, 37(7): 3082–3097. https://doi.org/10.1002/joc.4901

van Pelt WJJ, Kohler J, Liston GE, Hagen JO, Luks B, Reijmer CH, Pohjola VA (2016) Multidecadal climate and seasonal snow conditions in Svalbard. J Geophys Res Earth Surf, 121(11): 2100–2117. https://doi.org/10.1002/2016JF003999

Przybylak R, Wyszyński P, Nordli Ø, Strzyżewski T. (2016) Air temperature changes in Svalbard and the surrounding seas from 1865 to 1920. Int J Clim, 36(8): 2899-2916. https://doi.org/10.1002/joc.4527

Reimer PJ, Austin WE, Bard E, Bayliss A, Blackwell PG, Ramsey CB, Butzin M, Cheng H, Edwards RL, Friedrich M, Grootes PM (2020) The IntCal20 Northern Hemisphere radiocarbon age calibration curve (0–55 cal kBP). Radiocarbon, 62(4): 725-757. https://doi.org/10.1017/RDC.2020.41

Rubensdotter L, Rosqvist G (2009) Influence of geomorphological setting, fluvial-, glaciofluvial-and mass-movement processes on sedimentation in alpine lakes. The Holocene, 19(4): 665–678. https://doi.org/10.1177%2F0959683609104042

Trouet V, Esper J, Graham NE, Baker A, Scourse JD, Frank DC (2009) Persistent Positive North Atlantic Oscillation Mode Dominated the Medieval Climate Anomaly. Science, 324(5923): 78–80. https://doi.org/10.1126/science.1166349

van der Bilt WG, Born A, Haaga KA (2019) Was Common Era glacier expansion in the Arctic Atlantic region triggered by unforced atmospheric cooling?. Quaternary Science Reviews. 222: 105860. https://doi.org/10.1016/j.quascirev.2019.07.042

Weltje GJ, Tjallingii R (2008) Calibration of XRF core scanners for quantitative geochemical logging of sediment cores: Theory and application. Earth Planetary Sci Letters 274(3-4): 423-438. https://doi.org/10.1016/j.epsl.2008.07.054

Werner J, Divine DV, Ljungqvist FC, Nilsen T, Francus P (2018) Spatio-temporal variability of Arctic summer temperatures over the past 2 millennia. Clim Past, 14: 527–557. https://doi.org/10.5194/cp-14-527-2018

Woelders L, Lenaerts JTM, Hagemans K, Akkerman K, van Hoof TB, Hoek WZ (2018) Recent climate warming drives ecological change in a remote high-Arctic lake. Sci Rep, 8: 1–8. https://doi.org/10.1038/s41598-018-25148-7

Wolfe AP, Cooke CA, Hobbs WO (2006) Are current rates of atmospheric nitrogen deposition influencing lakes in the eastern Canadian Arctic? Arct Antarct Alp Res, 38(3): 465–476. https://doi.org/10.1657/1523-0430(2006)38[465:ACROAN]2.0.CO;2

Wolfe AP, Hätling JW (1997) Early holocene trace metal enrichment in organic lake sediments, Baffin Island, Arctic Canada. Arct Alp Res, 29(1): 24–31. https://doi.org/10.1080/00040851.1997.12003212

Xu H, Liu B, Wu F (2010) Spatial and temporal variations of Rb/Sr ratios of the bulk surface sediments in Lake Qinghai. Geochem Trans, 11 (3): 1–8. https://doi.org/10.1186/1467-4866-11-3

Yang Z, Zhang Y, Xie Z, Wang J, Li Z, Li Y, Du J, Sun L (2021) Potential influence of rapid climate change on elemental geochemistry distributions in lacustrine sediments—A case study at a high Arctic site in Ny-Ålesund, Svalbard. Sci Total Environ 801: 149784. https://doi.org/10.1016/j.scitotenv.2021.149784

Tables

Table 1: Results of ^{210}Pb dating and radiocarbon dated samples from the Blokkvatnet cores. ^{210}Pb dates were analysed from core BV1 and the ^{14}C date from core BV2.

Depth (cm) on BV1 (tuned depth for core BV2)	Age (AD ± error)	Dating method	Material	Sedimentation Rate (^{210}Pb dates only on core BV1) (g cm^{-2} yr^{-1})
0.13 (0.13)	2007 ± 1	^{210}Pb	Bulk sediment	0.029
0.38 (0.38)	2004 ± 1	^{210}Pb	Bulk sediment	0.027
0.63 (0.63)	2000 ± 1	^{210}Pb	Bulk sediment	0.025
0.88 (0.88)	1996 ± 2	^{210}Pb	Bulk sediment	0.026
1.13 (1.13)	1991 ± 2	^{210}Pb	Bulk sediment	0.027
1.38 (1.38)	1986 ± 3	^{210}Pb	Bulk sediment	0.024
1.63 (1.63)	1981 ± 3	^{210}Pb	Bulk sediment	0.021
1.88 (1.88)	1975 ± 4	^{210}Pb	Bulk sediment	0.021
2.13 (2.13)	1969 ± 5	^{210}Pb	Bulk sediment	0.021
2.38 (2.38)	1962 ± 6	^{210}Pb	Bulk sediment	0.021
2.63 (2.63)	1955 ± 6	^{210}Pb	Bulk sediment	0.021
2.88 (2.93)	1946 ± 7	^{210}Pb	Bulk sediment	0.026
3.13 (3.35)	1937 ± 8	^{210}Pb	Bulk sediment	0.031
3.38 (3.92)	1931 ± 8	^{210}Pb	Bulk sediment	0.054
3.63 (4.47)	1926 ± 8	^{210}Pb	Bulk sediment	0.078
3.88 (4.76)	1920 ± 9	^{210}Pb	Bulk sediment	0.052
4.13 (4.92)	1915 ± 9	^{210}Pb	Bulk sediment	0.027
4.38 (5.06)	1904 ± 10	^{210}Pb	Bulk sediment	0.024
4.63 (5.20)	1894 ± 10	^{210}Pb	Bulk sediment	0.021

4.88 (5.35)	1882 ± 11	^{210}Pb	Bulk sediment	0.021
5.13 (5.51)	1869 ± 12	^{210}Pb	Bulk sediment	0.021
Depth on BV2: 20.3 (19.9 – 20.7)	**AMS ^{14}C age:** 1480 ± 70 **Calibrated age** **(2σ age range):** 1440 (1310-1630)	AMS ^{14}C	Organic material	N/A

Table 2: Loadings of the variables for PC1 and PC2, following Principal Component Analysis on core BV1.

Element	PC1	PC2
Si	-0.21804	0.495157
Al	-0.74057	-0.16683
Mg	-0.62497	0.391353
Ca	0.218718	0.732688
Na	-0.18085	0.606062
K	-0.63159	0.123957
P	-0.16518	-0.66643
Rb	-0.81738	0.244213
Sr	-0.06936	-0.29519
Ti	-0.59867	0.629992
Zr	-0.92861	-0.16856
Fe	0.571399	0.412424
Mn	0.451386	-0.66051
S	0.761969	-0.19064
As	0.892815	-0.13665
Pb	0.30752	0.756068
Co	-0.25864	-0.55392
Cr	0.261675	-0.42226
Cu	-0.12053	0.449288
Ni	0.532553	-0.47558
Zn	-0.45165	0.786425
$\delta^{15}N$	0.551938	0.424011

N	0.701106	0.575284
$\delta^{13}C$	-0.7892	-0.24969
TOC	0.584191	0.751473

Figure Captions:

Figure 1: Location of lake Blokkvatnet. a) Map of Svalbard showing the study area (red rectangle) on Prins Karls Forland. Numbered points show the location of places mentioned within the text: 1) Longyearbyen, 2) Ny-Ålesund, 3) Holtedahlfonna glacier, 4) Austfonna ice cap. b) Map showing the location of Blokkvatnet in relation to topographic and hydrological features.

Figure 2: The two age-depth models developed for the BV1 and BV2 cores (left) and the BV2 core image and stratigraphy (right). The modelled median ages for BV1 and BV2 are shown by the orange and black lines respectively. The dashed lines showing the 2-sigma modelled confidence range for the BV2 age model. ^{210}Pb dates (at the original and tuned depths for BV1 and BV2 respectively) and the associated age uncertainties are shown for each core, along with the calibrated AMS radiocarbon date and 2-sigma range of uncertainty, which was only used for the core BV2 age model.

Figure 3: Organic parameters measured on cores BV1 (orange lines) and BV2 (black lines).

Figure 4: Concentrations of selected elements along core BV1 (orange lines) and BV2 (black lines). The BV1 element concentrations were analysed by XRF analysis, while the BV2 elements have been measured by an ITRAX XRF core scanner and are expressed as log-ratios. Plots of all the measured elements are presented in ESM3.

Figure 5: Principal Component Analysis of the organic parameters and element concentrations measured on core BV1. a) The loading of each variable for the first and second Principal Components. b) The PC1 (black line) and PC2 (blue line) eigenvector loadings over time for core BV1. c) Filtered mean seasonal air temperature records from Longyearbyen airport (Norwegian Meteorological Institute, 2022).

Figure 6: Comparison of the PC1 and TOC records for cores BV1 and BV2 respectively with selected palaeoclimate reconstructions. a) the TOC (%) record for core BV2 including the 2-sigma confidence range for the timing of the peaks in TOC (black line) and the eigenvector loading of PC1 along core BV1 (orange line), b) the reconstructed North Atlantic Oscillation index derived from reconstructed precipitation and drought records from Scotland and Morocco respectively (Trouet et al. 2009), c) Austfonna ice core $\delta^{18}O$ record (Isaksson et al. 2003). Shaded rectangles highlight intervals with inferred increases in organic matter deposition in BV1.

Figure 7: Comparison of selected variables with strong PC2 loadings along cores BV1 (a) and BV2 (b). The records have been standardised to aid comparison between the variables. The bottom plot (c) shows the average deviation of the upper and lower 2-sigma confidence range from the median age estimate along each core.

Figures:

Figure 1:

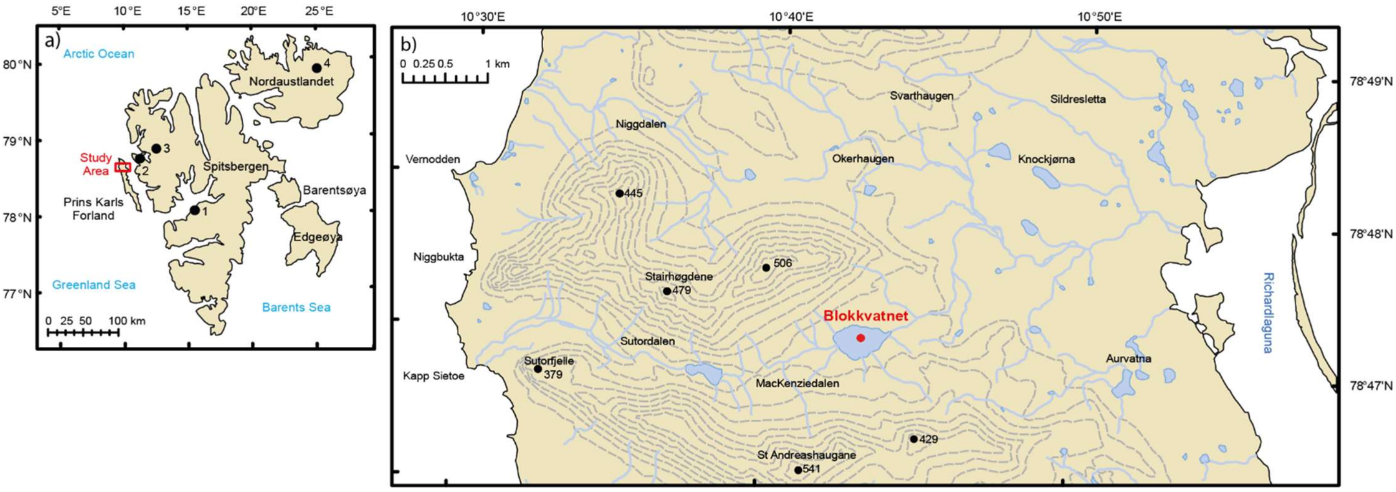
a)
5°E
10°E
15°E
20°E
25°E
80°N
79°N
78°N
77°N
Arctic Ocean
Nordaustlandet
Study Area
Spitsbergen
Barentsøya
Prins Karls Forland
Edgeøya
Greenland Sea
Barents Sea
0 25 50 100 km
1
2
3
4
b)
10°30'E
10°40'E
10°50'E
78°49'N
78°48'N
78°47'N
0 0.25 0.5 1 km
Svarthaugen
Sildresletta
Niggdalen
Vernodden
Okerhaugen
Knockjørna
445
Niggbukta
506
Stairhøgdene
479
Blokkvatnet
Richardlaguna
Sutordalen
Sutorfjelle
379
Kapp Sietoe
MacKenziedalen
Aurvatna
429
St Andreashaugane
541

Figure 2:

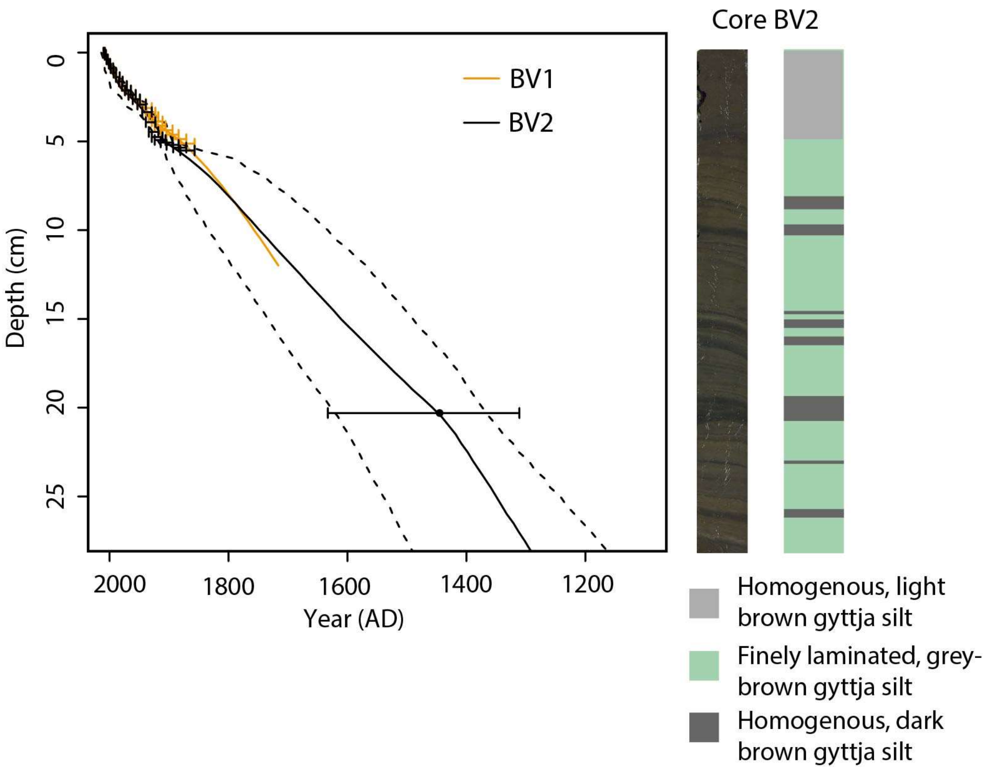
Core BV2
BV1
BV2
Depth (cm)
0
5
10
15
20
25
2000
1800
1600
1400
1200
Year (AD)
Homogenous, light brown gyttja silt
Finely laminated, grey-brown gyttja silt
Homogenous, dark brown gyttja silt

Figure 3:

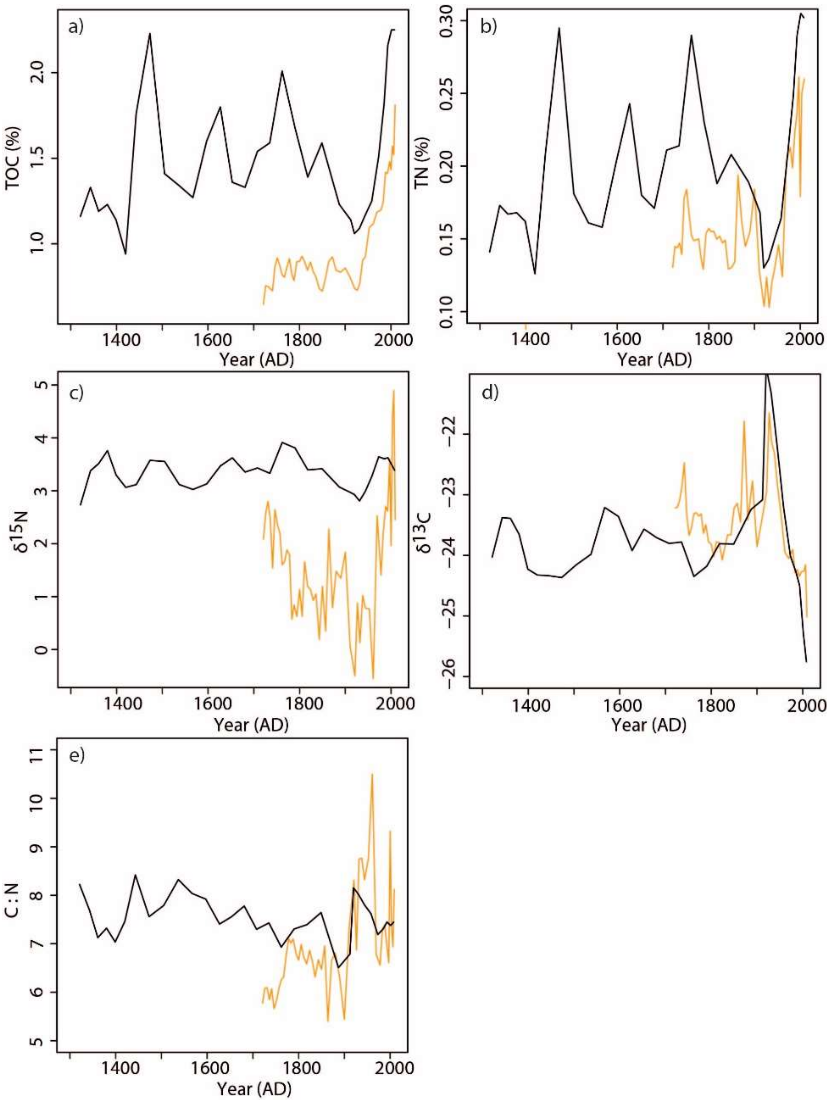
a)
TOC (%)
Year (AD)
b)
TN (%)
Year (AD)
c)
δ15N
Year (AD)
d)
δ13C
Year (AD)
e)
C : N
Year (AD)

Figure 4:

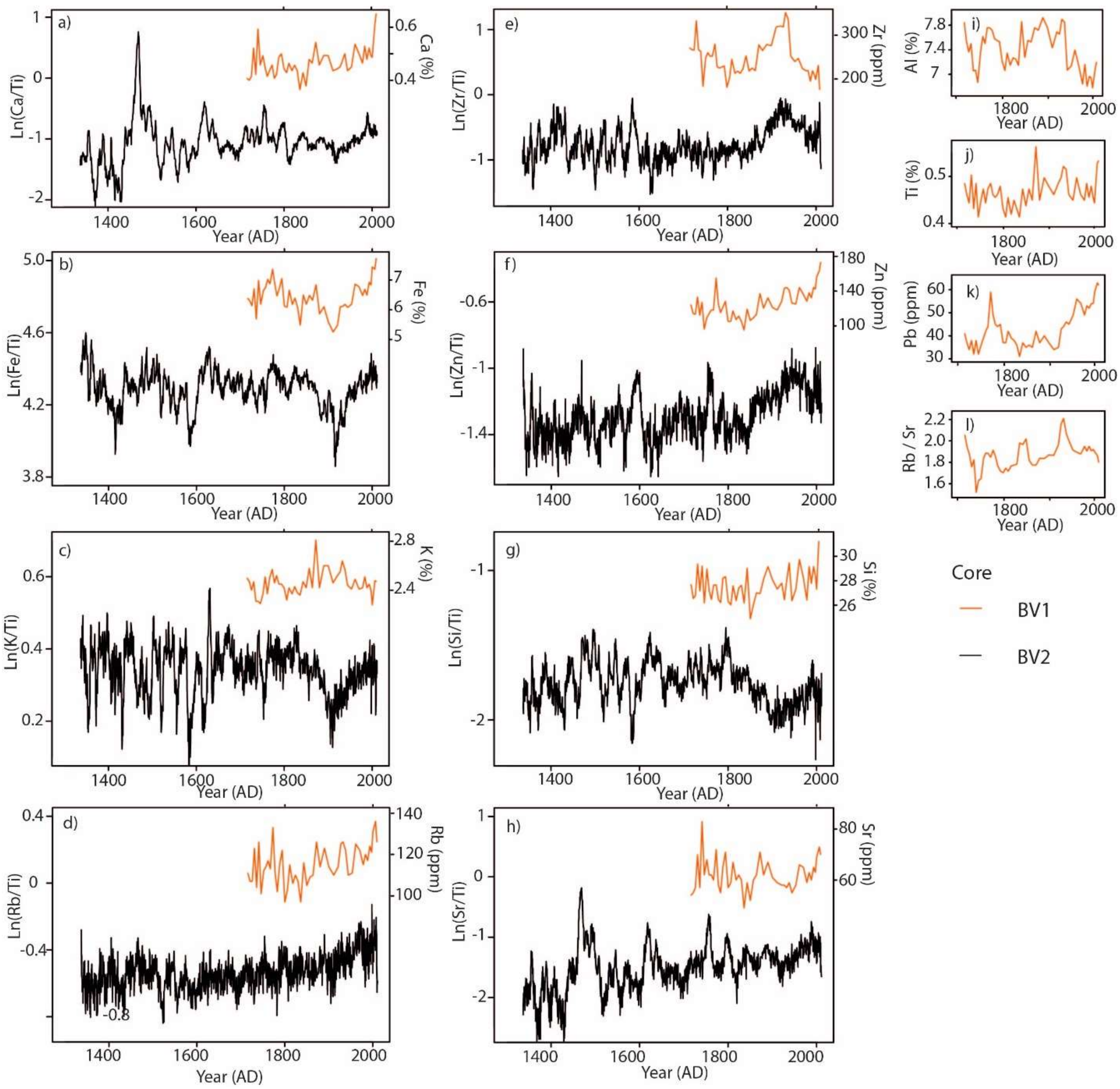

a)
Ln(Ca/Ti)
Ca (%)
b)
Ln(Fe/Ti)
Fe (%)
c)
Ln(K/Ti)
K (%)
d)
Ln(Rb/Ti)
Rb (ppm)
e)
Ln(Zr/Ti)
Zr (ppm)
f)
Ln(Zn/Ti)
Zn (ppm)
g)
Ln(Si/Ti)
Si (%)
h)
Ln(Sr/Ti)
Sr (ppm)
i)
Al (%)
j)
Ti (%)
k)
Pb (ppm)
l)
Rb / Sr
Year (AD)
Core
BV1
BV2

Figure 5:

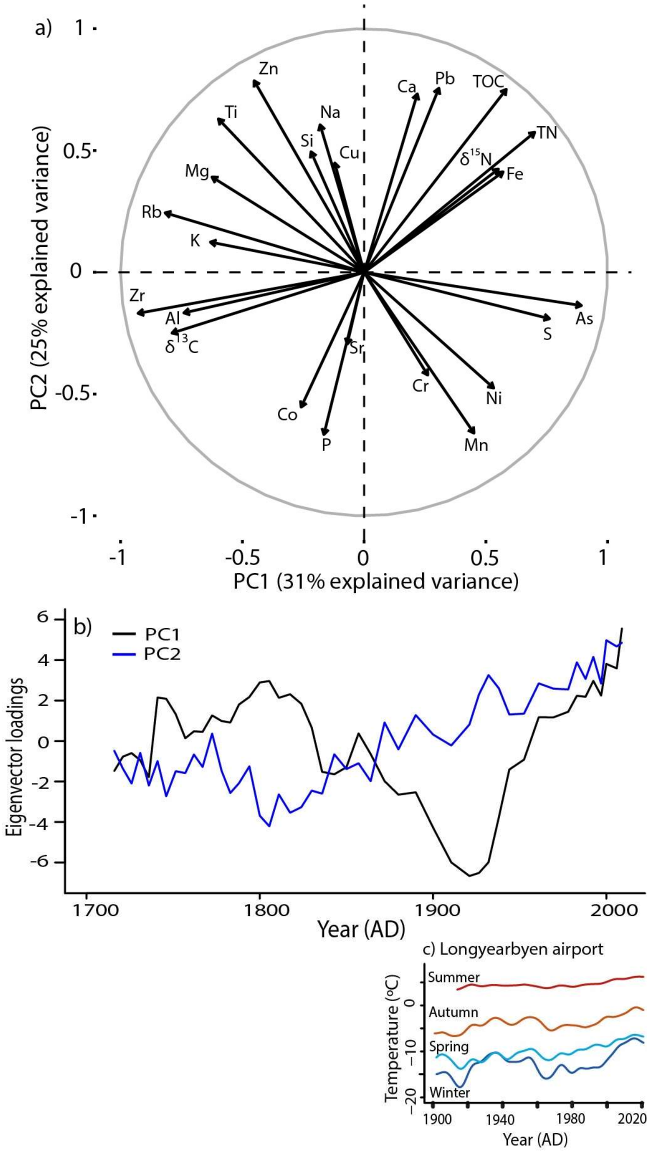

a)
PC1 (31% explained variance)
PC2 (25% explained variance)
Zn
Ti
Na
Si
Cu
Mg
Rb
K
Ca
Pb
TOC
TN
δ15N
Fe
Zr
Al
δ13C
Sr
Co
P
Cr
Ni
Mn
S
As
b)
PC1
PC2
Eigenvector loadings
Year (AD)
c) Longyearbyen airport
Summer
Autumn
Spring
Winter
Temperature (°C)
Year (AD)

Figure 6:

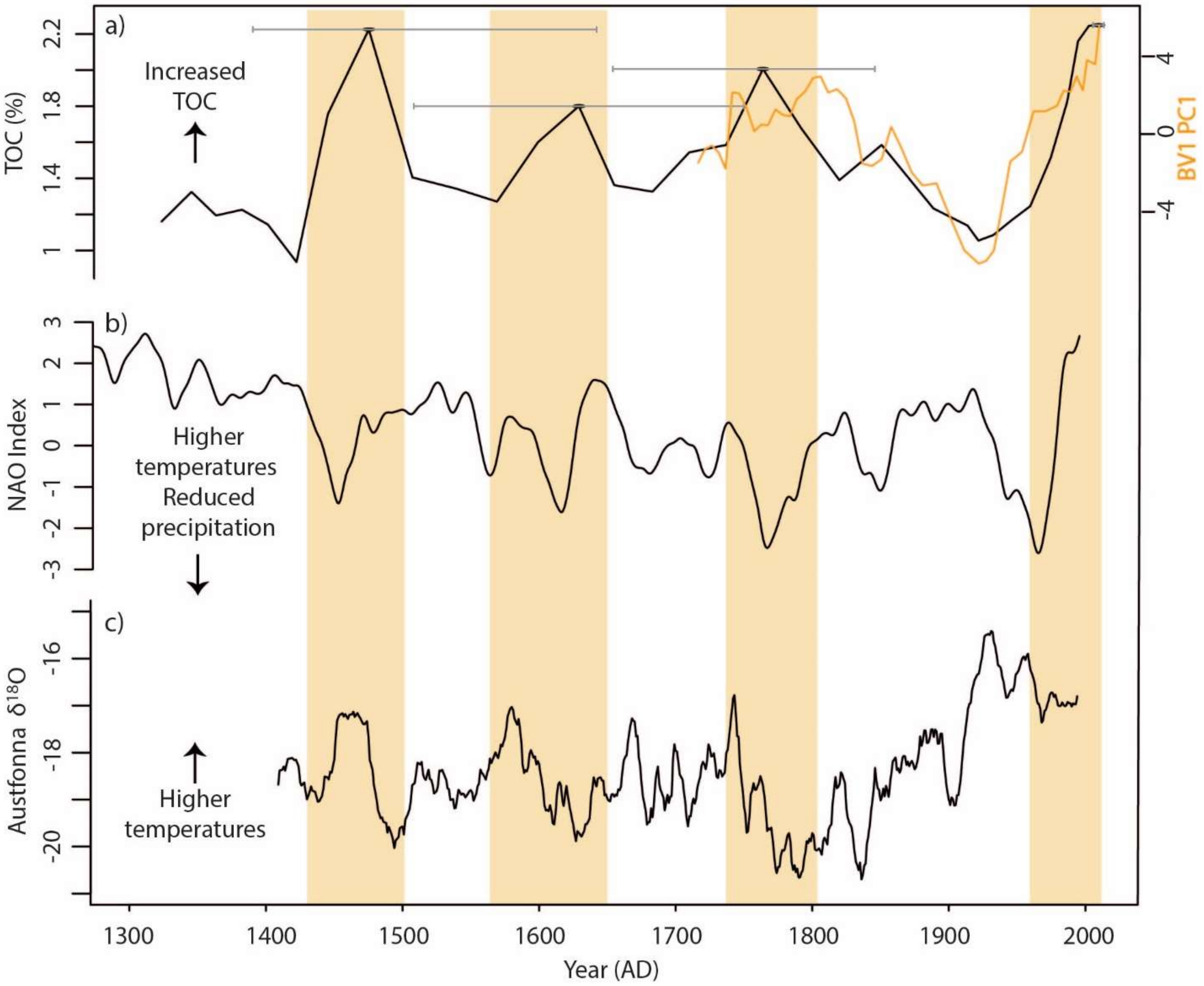
a)
Increased
TOC
TOC (%)
BV1 PC1
b)
NAO Index
Higher
temperatures
Reduced
precipitation
c)
Austfonna δ18O
Higher
temperatures
Year (AD)

Figure 7:

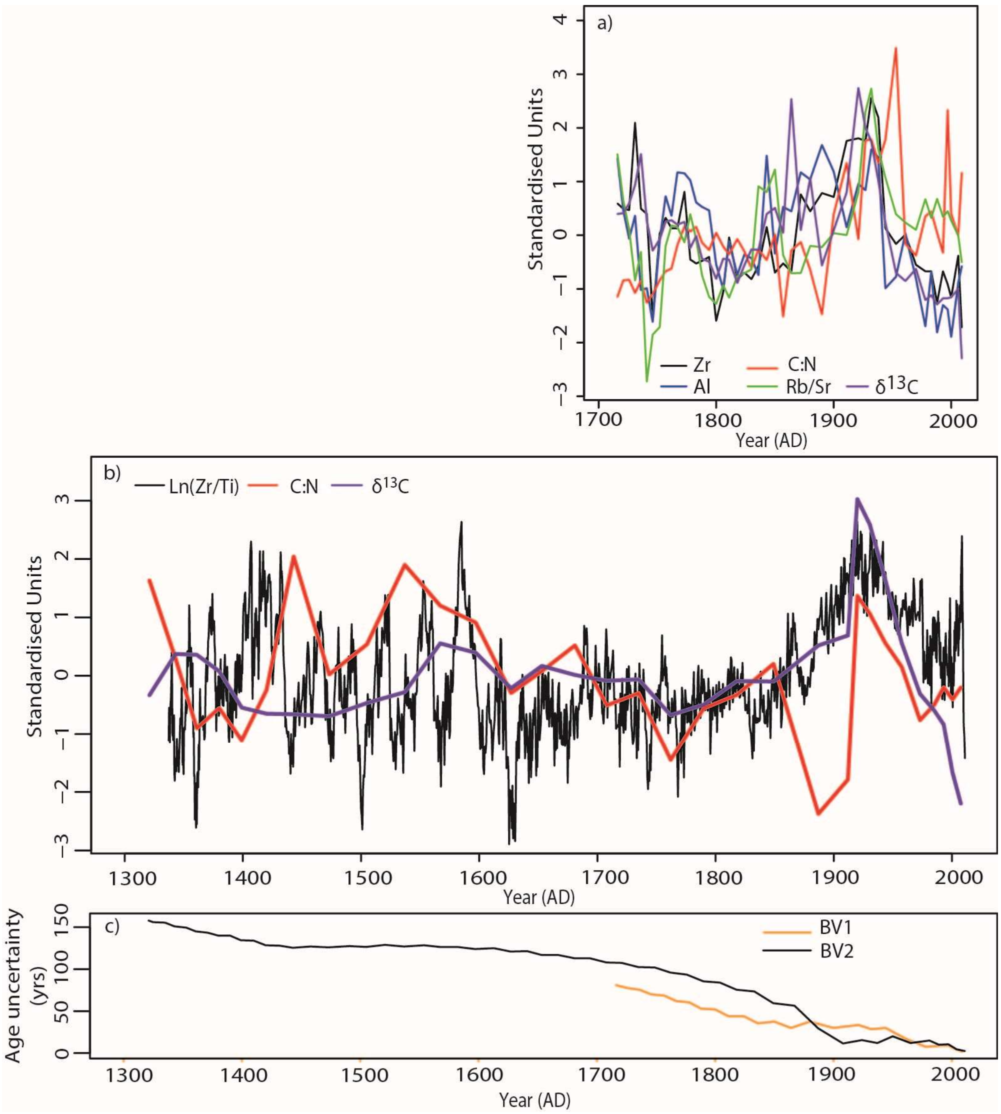
a)
Standardised Units
Zr
Al
C:N
Rb/Sr
δ13C
Year (AD)
b)
Ln(Zr/Ti)
C:N
δ13C
Standardised Units
Year (AD)
c)
BV1
BV2
Age uncertainty (yrs)
Year (AD)